Coordinated Planning Strategy for Integrated Energy Systems in a District Energy Sector

Wentao Yang, *Student Member, IEEE*, Weijia Liu, Chi Yung Chung, *Fellow, IEEE*, and Fushuan Wen, *Senior Member, IEEE*

***Abstract*—With the ever-growing integration of diverse distributed energy resources, modern district energy sectors are transitioning into integrated energy systems (IESs), which generally consist of various energy carriers such as electric power, natural gas, and heat. Instead of modeling individual energy carriers, the emergence of IESs requires comprehensive consideration of all involved energy systems in both planning and operation phases. This paper proposes a comprehensive planning strategy for a district energy sector to address the challenges of IES planning considering the coupling of power, gas, and heat systems. The proposed planning model contains an operational module that develops a steady-state optimal multi-energy flow (OMEF) for the IES considered and a multi-stage expansion module that optimizes the investment decisions. To efficiently solve the proposed planning model, which is formulated as a mixed-integer nonlinear programming problem, an improved generalized Benders decomposition algorithm that utilizes dynamic dual multipliers to improve the convergence speed is employed. The effectiveness of the proposed planning model and the feasibility of the improved Benders decomposition algorithm are verified in case studies.**

***Index Terms*—Coordinated planning, district energy sector, integrated energy systems, improved generalized Benders decomposition, optimal multi-energy flows.**

NOMENCLATURE

Acronyms

CHP	Combined heat and power
DHS	District heating system
GBD	Generalized Benders decomposition
GDS	Gas distribution system
IES	Integrated energy system
MIQCP	Mixed-integer quadratically constrained program
OMEF	Optimal multi-energy flow
P2G	Power to gas
PDS	Power distribution system
O&M	Operation & maintenance

Sets and Indexes

$\Omega^P/u, v$	Set and indexes of buses
$\Omega^G/w, q$	Set and indexes of natural gas nodes
$\Omega^L/j, l$	Set and indexes of heat pipes
$\Omega^W/k, \Omega^H/i$	Sets and indexes of gas pipes, heat nodes
Γ/τ	Set and index of planning stages
$\Omega^{PS}, \Omega^{GS}, \Omega^{HS}$	Sets of PDS, GDS, and DHS schemes
$\Omega^{EB}, \Omega^{P2G}, \Omega^{CHP}$	Sets of boiler, P2G, and CHP schemes
$\Omega^{NP\tau}$ $(\Omega^{P\tau})$, $\Omega^{NW\tau}$, $(\Omega^{W\tau})$ $\Omega^{NL\tau}$ $(\Omega^{L\tau})$	Sets of candidate (existing) buses, gas pipes, and heat-pipes

Variables and Parameters of OMEF Model

$A^P_{u,v}, A^G_{q,k}, A^H_{i,l}$	Elements of the adjacent matrix in a PDS, GDS, and DHS
c, ρ	Specific heat capacity and density of water
$D_{l,t}, L_l, d_l$	Length, mass flow, inner diameter of pipe l
f_t^{OMEF}	Operational cost at the t-th interval
$G_{w,t}/G_{q,t}$	Nodal gas pressure of node w/q
M_k	Parameter of gas pipe k
$p_{i,t}$	Water pressure of heat node i
$P^S_{u,t}, F^S_{q,t}$	Purchased electric power and natural gas
$P^{EB}_{u,t}/P^{EB}_{l,t}$	Electric load of the boiler
$P^{P2G}_{q,t}/P^{P2G}_{u,t}$	Electric load of P2G station
$P^{CHP}_{l,t}/P^{CHP}_{u,t}$	Electric output of the CHP plant
$P^{WP}_{u,t}/P^{WP}_{l,t}$	Electric load of the water pump
$P^L_{u,t}(Q^L_{u,t}), F^L_{q,t}, \Phi^L_{l,t}$	Active (reactive) electric power load, natural gas load, and heat load
$\Delta P_{u,t}$	Power loss of feeder whose power receiving node is bus u
Δt	Length of each operation interval
T^0_t	Environmental temperature at time t

Manuscript received March 26, 2019; revised August 1, 2019; accepted September 8, 2019. Date of publication September 13, 2019; date of current version June 19, 2020. This work was supported in part by the Natural Sciences and Engineering Research Council (NSERC) of Canada and the Saskatchewan Power Corporation (SaskPower), in part by National Key Research and Development Program of China (Basic Research Class) under Grant 2017YFB0903000, and in part by National Natural Science Foundation of China under Grant U1509218. This work was authored in part by the National Renewable Energy Laboratory, operated by Alliance for Sustainable Energy, LLC, for the USA Department of Energy (DOE) under Contract no. DE-AC36-08GO28308. Paper no. TSTE-00341-2019 *(Corresponding author: C. Y. Chung.)*

W. Yang is with the College of Electrical Engineering, Zhejiang University, Hangzhou 310027, China, and also with the Department of Electrical and Computer Engineering, University of Saskatchewan, Saskatoon, SK S7N 5A9, Canada (e-mail: wentaoyang@zju.edu.cn).

W. Liu is with the Power System Engineering Center, National Renewable Energy Laboratory, Golden, CO 80401 USA (e-mail: liuweijiamarcel@gmail.com).

C. Y. Chung is with the Department of Electrical and Computer Engineering, University of Saskatchewan, Saskatoon, SK S7N 5A9, Canada (e-mail: c.y.chung@usask.ca).

F. Wen is with the College of Electrical Engineering, Zhejiang University, Hangzhou 310027 China, and also with the Department of Electrical Power Engineering and Mechatronics, Tallinn University of Technology, Tallinn 12616, Estonia (e-mail: fushuan.wen@gmail.com).

Color versions of one or more of the figures in this article are available online at http://ieeexplore.ieee.org.

Digital Object Identifier 10.1109/TSTE.2019.2941418

$V_{u,t}$, V_B	Time-varied voltage and reference value
V,$\overline{V}$	Upper and lower limits of voltage magnitude
η_e^{CHP}, η_h^{CHP}	Electric and heat output efficiency of CHP
η^{P2G}, η^{EB}, η^{WP}	Efficiencies of P2G, boiler, and water pump
θ_P, θ_G, θ_H	Unit O&M costs of boiler, P2G, and CHP
κ, Υ	Heat transfer coefficient and friction factor
π	Mathematical constant pi
φ_P, φ_G, φ_H	Prices of electricity, natural gas, and heat
$\Delta\Phi_{l,t}$, $\Delta p_{l,t}$	Heat loss and pressure drop of heat pipe l

Variables and Parameters of Expansion Investment Model

c_1^G, c_2^G c_2^G, c_3^G	Cost coefficients of new gas pipe installment, existing gas pipe reinforcement, and P2G investment
c_1^H, c_2^H, c_3^H	Cost coefficients of new heat pipe installment, existing heat pipe reinforcement, and CHP investment
c_1^P, c_2^P, c_3^P	Cost coefficients of bus installation/reinforcement, new feeder installation, and electric boiler investment
D_c, P_c^{CHP}	Installed/reinforced capacity of heat pipe and capacity of CHP plant in the scheme c
f^{Expa}	Total expansion cost
$f^{P\tau}$, $f^{G\tau}$, $f^{H\tau}$	Sub-costs of PDS, GDS, and DHS
F_b, P_b^{P2G}	Installed/reinforced capacity of gas pipes and capacity of P2G plant in the scheme b
S_a, $\Re_a$, P_a^{EB}	Installed/reinforced capacity, construction plan (length and type) of feeder, and electric power load of boiler in the scheme a, with their unit costs
$x_{u,a}^{P\tau}$, $x_{k,b}^{G\tau}$, $x_{l,c}^{H\tau}$	Binary variables of constructing new feeders/pipes whose receiving end are bus u, gas node k, and heat node l
$\boldsymbol{x}$, $\boldsymbol{y}$, $\boldsymbol{z}$	Matrixes of binary variables in planning
$y_{u,a}^{P\tau}$, $y_{k,b}^{G\tau}$, $y_{l,c}^{H\tau}$	Binary variables of reinforcing existing feeders/pipes whose receiving end are bus u, gas node k, and heat node l
$z_{u,a}^{P\tau}$, $z_{q,b}^{G\tau}$, $z_{l,c}^{H\tau}$	Binary variables of constructing the boiler, P2G station, and CHP plant at PDS bus u, gas pipe k, and heat pipe l
γ	Interest rate

I. Introduction

With the gradual depletion of fossil energy, renewable energy generation resources, mainly solar and wind power, have received extensive attention [1], [2]. To promote the utilization of renewable energy as well as enhance the efficiency of end-use energy consumption, the coupling devices, i.e., combined heat and power (CHP) plants [3], power to gas (P2G) stations [4], and electric boilers [5], are widely integrated into district energy sectors. Because these devices consume/generate energy in different forms, the interconnections of different energy carriers, especially in energy distribution systems, have been strengthened more than ever before [6]. Thus, it is important to comprehensively study the influences of integrated energy systems (IESs) on the transition of district energy sectors.

Plenty of works have been done so far to address coordinated planning strategies for integrated power distribution systems (PDSs) and gas distribution systems (GDSs). A chance-constrained programming approach is presented in [7] to meet stochastic energy demands and highlight the role of natural gas storage in managing short-time uncertainties. A novel multi-stage stochastic programming model considering the uncertainties in net load demand is proposed in [8]. Meanwhile, [9] uses a two-stage stochastic optimization model to address the coordinated planning, which provides a tradeoff between accuracy and computational tractability. A bi-level multi-stage programming problem is formulated to minimize the cost in [10], where gas-fired power generation and P2G stations are considered. Coordinated planning considering district heating systems (DHSs) has also been explored. [11] investigates the problem of integrated planning for a large-scale heat pump to optimally link electric and heat utilities. An optimal co-planning model is established in [12] to minimize the investment cost of coupling equipment as well as the operation energy consumption of IESs. In [13], a two-stage approach considering distributed renewable energy integration is presented, where coupling devices are optimally selected.

However, due to the absence of an effective steady-state multi-energy flows model, the expansion planning of DHSs is too complex to be integrated into existing models that already consider PDSs and GDSs. Thus, the issue of optimizing heat-pipe type and DHS topologies remains relatively unexplored in coordinated planning problems. According to [14], how to determine the optimal parameters of heat pipes (e.g., length, inner diameter, material, etc.) are key issues in heating-related disciplines. Although well-established methods such as the dynamic method [15], [16] and the Kirchhoff-based steady-state method [17], [18] are available to analyze the DHSs, they cannot be effectively implemented in the planning of DHSs because of the following drawbacks: 1) the dynamic method is described by a set of partial differential equations, which is time-consuming to solve and difficult to integrate into the planning model; 2) the Kirchhoff-based steady-state method cannot effectively account for energy losses related to heat pipes, making this method infeasible for the planning of heat pipes in DHSs because the cost of energy losses is a vital index when searching for the optimal planning candidate [12]; 3) both methods must be solved by an interactive Newton-Raphson method [6], which is difficult to be optimized using the efficient commercial solvers; and 4) both models are divided into thermal and hydraulic submodels for simplification while ignoring the physical coupling between heat and pressure. As a result, the dynamic method and Kirchhoff-based steady-state method are not feasible to integrate

the planning of DHS into the coordinated planning framework of IESs.

To tackle these weaknesses, a steady-state energy flow model is proposed for the DHS. In this model, the term *heat flow* is proposed to describe the mass flow of hot water with heat energy and water pressure as the state variables. The impacts of heat pipe parameters and environmental temperature on heat energy loss and pressure drop are also considered. Combining the proposed heat flow with electricity and natural gas flows [19], a comprehensive optimal multi-energy flow (OMEF) model is derived to analyze the planning and operation of IESs.

In addition, this paper also addresses methods to reduce the computational burden of coordinated planning. The expansion planning models for energy systems with a single carrier (e.g., power system) are generally formulated as a mixed-integer quadratically constrained program (MIQCP) problem, which is difficult to solve efficiently. To make matters worse, the planning model for IESs is more complicated because three different energy carriers with diverse characteristics are considered. Hence, directly solving the MIQCP planning model for IESs is expected to be very time-consuming. The generalized Benders decomposition (GBD) is widely adopted to solve complex problems such as MIQCP problems by decomposing the original model into several sub-problems and solving them in an iterative fashion [20], [21]. But, the dual multiplier values significantly affect the generation of Benders cuts and the convergence speed. Thus, this paper also attempts to develop an improved GBD method to dynamically update the dual multipliers for faster convergence.

In summary, the contributions of this paper mainly include:

- proposing a steady-state OMEF method to analyze multi-energy flows that consider the impacts of heat pipe parameters to pipe type and DHS topology in coordinated planning;
- developing a multi-stage coordinated planning strategy for IESs that not only optimizes coupling devices but also considers topology expansion; and
- proposing an improved GBD algorithm to improve the computational efficiency of MIQCP model.

The rest of this paper is organized as follows. The planning problem of an IES is briefly described in Section II. The OMEF and the coordinated planning models are respectively proposed in Sections III and IV. The improved GBD algorithm is discussed in Section V. Case studies and numerical results are presented in Section VI. Finally, conclusions are given in Section VII.

II. Problem Description

In this paper, the typical district IES consists of three subsystems, i.e., the PDS, GDS, and DHS. It is also assumed that all sub-systems are owned and operated by the same entity, for example, the district IES in industrial parks or universities [6]. Among them, the PDS and GDS both generally operate radially [22]. On the contrary, the DHS usually adopts a looped structure and two symmetric networks, i.e., the water supply and return networks. However, due to its symmetry, the looped DHS also can be shown as a radial system, as presented in [23], [24]. The same manner will be adopted in this paper, as illustrated in Fig. 1.

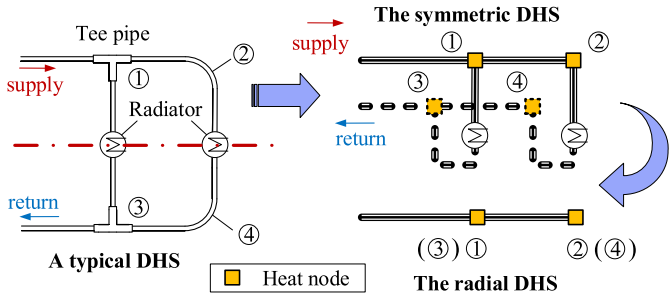

Fig. 1. Illustration of a typical DHS.

TABLE I
Optimization Variables of the Coordinated Planning

System	Binary variables	Continuous	
		operation	decision
PDS	$\boldsymbol{x}^P, \boldsymbol{y}^P, \boldsymbol{z}^P$	V: voltage P, Q: active and reactive power flows	P^{EB}: boiler consumption P^S, Q^S: injected active and reactive powers
GDS	$\boldsymbol{x}^G, \boldsymbol{y}^G, \boldsymbol{z}^G$	G: natural gas pressure F: natural gas flow	F^S: injected natural gas P^{P2G}: P2G consumption
DHS	$\boldsymbol{x}^H, \boldsymbol{y}^H, \boldsymbol{z}^H$	Φ: unit heat energy of hot water [kW] p: water pressure D: mass flow	P^{CHP}: electric power output of CHP plant P^{WP}: consumption of water pump

In Fig. 1, the typical DHS is folded up to a radial structure based on its symmetry. Dual heat nodes at the same position, such as ① and ③, can be combined. Thus, each node in a radial DHS represents two dual heat nodes in supply and return heat pipes, respectively.

Three kinds of coupling devices, namely the CHP plant, P2G station, and electric boiler, are considered in the IES planning to promote closed-loop energy flows. For instance, the CHP plant consumes natural gas to produce electric power and heat, whereas the P2G station and electric boiler consume electric power to produce natural gas and heat, respectively. To clearly address the coordinated planning problem, the variables involved are listed in Table I.

In Table I, the binary variables are optimized in the expansion sub-model to determine the investment decisions related to installing/reinforcing devices over the planning stages. $\boldsymbol{x}^P$ ($\boldsymbol{y}^P$), $\boldsymbol{x}^G$ ($\boldsymbol{y}^G$), and $\boldsymbol{x}^H$ ($\boldsymbol{y}^H$) denote the planning decisions related to constructing new (reinforcing existing) distribution buses, heat pipes, and gas pipes, respectively. $\boldsymbol{z}^P$, $\boldsymbol{z}^G$, and $\boldsymbol{z}^H$ denote the investment decisions related to CHP plants, P2G stations, and electric boilers, respectively. The continuous variables are optimized by the operating sub-model, i.e., the OMEF model, to examine the feasibility of candidate planning schemes.

In the following sections, the coordinated planning problem will be established from two aspects, i.e., the optimal OMEF model and the expansion investment model.

III. Optimal Multi-Energy Flows Model

A. Objective Function

The objective of the OMEF model, denoted as f_t^{OMEF}, is established to minimize operational costs as follows.

$$\begin{aligned}\min f_t^{\mathrm{OMEF}} = & \sum_{u\in\Omega^P}\left[\varphi_P\left(P_{u,t}^S+\Delta P_{u,t}\right)+\theta_P\sum_{u\in\Omega^P}P_{u,t}^{EB}\right]\Delta t \\ & +\sum_{q\in\Omega^G}\left(\varphi_G F_{q,t}^S+\theta_P P_{q,t}^{P2G}\right)\Delta t \\ & +\sum_{l\in\Omega^L}\left(\varphi_H\Delta\Phi_{l,t}+\theta_H P_{l,t}^{CHP}\right)\Delta t \end{aligned} \tag{1}$$

In (1), f_t^{OMEF} consists of three terms: 1) costs of purchasing electricity, power loss, and boiler operation & maintenance (O&M) [25] in PDS; 2) costs of purchasing natural gas and P2G station O&M in GDS; and 3) costs of heat loss and CHP plant O&M in the DHS.

B. Constraints of the PDS

As a well-established method for analyzing the PDSs [26], Distflow makes full use of the radial structure by combining the variables in each feeder, e.g., $\Delta P_{u,t}$, with those at its power receiving node [26]. Note that the power loss is approximated by a relaxed form shown in (3) to guarantee the convexity of the power flow constraints. This approximation has been validated by studies such as [26] and is not further discussed due to space limitation. The constraints of Distflow, as respectively described by (2) and (3), are applicable to all PDS buses.

$$\begin{cases}\sum_{v\in\Omega^P}A_{u,v}^P P_{v,t}+P_{u,t}^S+P_{u,t}^{CHP}+P_{u,t}^{PV}+P_{u,t}^{Wind} \\ \quad =\Delta P_{u,t}+P_{u,t}^{EB}+P_{u,t}^{P2G}+P_{u,t}^{WP}+P_{u,t}^L \\ \sum_{v\in\Omega^P}A_{u,v}^P Q_{v,t}+Q_{u,t}^S=Q_{u,t}^L\end{cases} \tag{2}$$

$$\begin{cases}-\overline{P_u}\le P_{u,t}\le\overline{P_u};\quad -\overline{Q_u}\le Q_{u,t}\le\overline{Q_u}; \\ \quad {P_{u,t}}^2+{Q_{u,t}}^2\le{\overline{S}_u}^2 \\ \Delta P_{u,t}\ge R_u\left({P_{u,t}}^2+{Q_{u,t}}^2\right)/{V_B}^2 \\ \underline{V}\le V_{u,t}\le\overline{V};\quad \sum_{v\in\Omega^P}A_{u,v}^P V_{u,t} \\ \quad =\left(R_u P_{u,t}+X_u Q_{u,t}\right)/V_B \\ 0\le P_{u,t}^S\le\overline{P}_u^S;\quad 0\le Q_{u,t}^S\le\overline{Q}_u^S\end{cases} \tag{3}$$

where $P_{u,t}$ ($Q_{u,t}$) and $P_{u,t}^S$($Q_{u,t}^S$) denote the active (reactive) electric power flow injection and purchased electric power of bus u at time t, which are limited to $\bar{P}_u(\bar{Q}_u)$ and $P_u^S(\bar{Q}_u^S)$, respectively; S_u, R_u, and X_u are respectively the apparent power capacity, resistance, and reactance of the feeder whose receiving end is u; $\bar{S}_u$ is the upper limit of S_u; $P_{u,t}^{PV}$ and $P_{u,t}^{Wind}$ are respectively the local photovoltaic and wind powers.

The active and reactive power balances are established in (2). The power flow constraints including power and capacity limit of feeders, power loss approximation, voltage magnitude limit, voltage drop equation, and power injection limit at source nodes are listed in (3).

C. Constraints of the GDS

The GDS models available mainly include dynamic models [27] and steady models [28]. While the dynamic gas flow focuses on the transient process of gas transmission, the steady gas flow equations are sufficient for planning and operating purposes. In addition, there are no gas compressor stations in GDSs because the size of a GDS is normally very small (gas pipes within several miles) and the pressure drop is not significant [22]. According to [29], natural gas only needs to be re-pressurized when the transmission distance is as long as 40 to 100 miles. Thus, the steady gas flow can be expressed by a relaxed convex model [28], as follows:

$$\sum_{k\in\Omega^W}A_{q,k}^G F_{k,t}+F_{q,t}^S+\eta^{P2G}P_{q,t}^{P2G}=F_{q,t}^L+P_{q,t}^{CHP}/\eta_e^{CHP} \tag{4}$$

$$\begin{cases}{F_{k,t}}^2={F_{wq,t}}^2\le M_k\left(G_{w,t}-G_{q,t}\right)+\psi\left(1-\varepsilon_{wq,t}\right) \\ {F_{wq,t}}^2\le\psi\varepsilon_{wq,t};\quad G_{w,t}-G_{q,t} \\ \quad\le\psi\varepsilon_{wq,t};\quad \varepsilon_{wq,t}\in\{0,1\} & \forall k\in\Omega^W \\ 0\le F_{k,t}\le\overline{F} \\ \underline{G}\le G_{q,t}\le\overline{G};\quad 0\le F_{q,t}^S\le\bar{F}_q^S\end{cases} \tag{5}$$

where $F_{k,t}$ is the natural gas flow of gas pipe k at time t, and is also represented by $F_{wq,t}$ when the sending end nodes of the gas pipe k are respectively w and q; F, G, and $\bar{F}_q^s$ denote respectively the upper limits of $F_{k,t}$, $G_{q,t}$, and $F_{q,t}^S$; ψ is a large positive number; and $\varepsilon_{wq,t}$ is the binary variable of natural gas flow direction, where $\varepsilon_{wq,t}=1$ when $G_{w,t}>G_{q,t}$ and 0 otherwise.

Equation (4) is established to balance the natural gas flow in each gas pipe. Equation (5) respectively includes the relaxed gas flow equation, gas flow direction constraints, gas flow limit, gas node pressure limit, and the source node gas injection limit.

D. Constraints of the DHS

In this work, the state variables of the DHS, i.e., heat energy and pressure of hot water, are holistically simulated in a mixed thermo-pressure field. Compared with existing methods such as hydraulic-thermal models that simulate thermal and hydraulic sub-models separately, the proposed heat model is more reasonable in terms of the consideration of physical coupling relationship of state variables. Referring to the lumped-parameter model of a transmission line [30], a steady-state model is proposed for heat pipes, as depicted below.

In Fig. 2, $\Phi_{i,t}\,(p_{i,t})$ and $\Phi_{j,t}\,(p_{j,t})$ are the inlet unit heat energy (pressure) from node i and outlet heat power (pressure) to node j, respectively; $\Phi_{x,t}\,(p_{x,t})$ denotes the unit heat energy (pressure) of the node that is x meters away from i; $d\Phi$ and dp respectively denote the heat loss and pressure drop after transferring through a length of dx; and z_0 and y_0 are the unit pressure resistance and thermal conductance of the heat pipe, respectively. For any heat pipe l, the lumped pressure resistance (Z) and thermal conductance (Y) can be calculated as follows

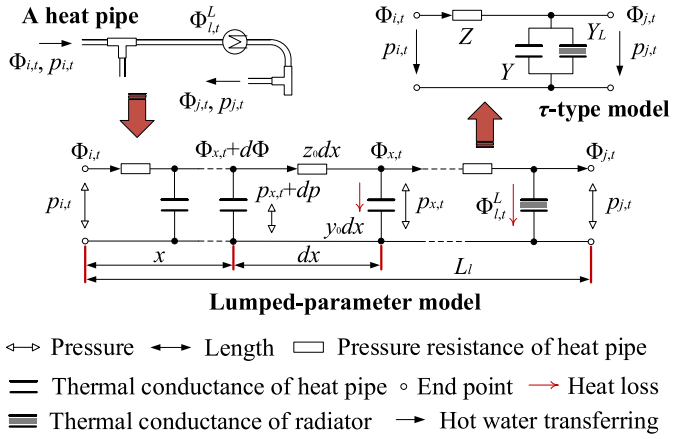

Fig. 2. Lumped-parameter steady-state model for a heat pipe.

[30]:

$$\begin{cases} Z = \sqrt{z_0/y_0}\sinh\sqrt{z_0 y_0}L_l \\ Y = 2\left(\cosh\sqrt{z_0 y_0}L_l - 1\right)\Big/\left(\sqrt{z_0/y_0}\sinh\sqrt{z_0 y_0}L_l\right) \end{cases} \tag{6}$$

$$z_0 = 8\Upsilon {D_{l,t}}^2/\left(\pi^2 {d_l}^5 \rho \Phi_{i,t}\right) \tag{7}$$

$$y_0 = \kappa\left(\Phi_{j,t}/c - D_{l,t}T_t^0\right)/\left(p_{j,t}L_l\right) \tag{8}$$

As shown in (8), y_0 is affected by $\Phi_{j,t}$ and $p_{j,t}$ at the same time, which verify the physical relationship between state variables. Note that the heat transfer coefficient and friction factor of pipe walls (κ and Υ) vary for different materials [31].

In (6), functions "sinh(•)" and "cosh(•)" are further expanded in Taylor series with nonlinear terms omitted. Thus, *Z* and *Y* can be reformulated as:

$$\begin{aligned} Z &= 8\Upsilon {D_{l,t}}^2 L_l/\left(\pi^2 {d_l}^5 \rho \Phi_{i,t}\right); \\ Y &= \kappa\left(\Phi_{j,t}/c - D_{l,t}T_t^0\right)/p_{j,t} \end{aligned} \tag{9}$$

Based on the simplified τ-type steady-state model in Fig. 2, the heat loss $(\Delta\Phi_{l,t})$ and pressure drop $(\Delta p_{l,t})$ of heat pipe l are respectively established as:

$$\begin{aligned} \Delta\Phi_{l,t} &= \left(Y_L + Y\right)p_{j,t} = \Phi_{l,t}^L + \kappa\left(\Phi_{i,t} - \Delta\Phi_{l,t}\right)/c - \kappa D_{l,t}T_t^0 \\ &\overset{\Phi_{i,t}=\Phi_{l,t}}{\Rightarrow} \Delta\Phi_{l,t} = \left(\Phi_{l,t}^L + \kappa\Phi_{l,t} - \kappa c D_{l,t}T_t^0\right)/\left(c+\kappa\right) \end{aligned} \tag{10}$$

$$\Delta p_{l,t} = Z\Phi_{i,t} = 8\Upsilon {D_{l,t}}^2 L_l/\left(\pi^2 {d_l}^5 \rho\right) \tag{11}$$

where $Y_L = \Phi_{l,t}^L/p_j$, is the thermal conductance of a radiator and $\Phi_{l,t} = \Phi_{i,t}$ is the inlet heat power of heat pipe l at time t.

As shown in (10), (11), $\Delta\Phi_{l,t}$ and $\Delta p_{l,t}$ are both calculated from the heat pipe parameters, i.e., the length (L_l), inner diameter (d_l), material (κ and Υ), and environmental temperature (T_t^0). In this manner, all of the parameters can be optimized in the planning problem to enable a DHS to operate with minimal heat loss and pressure drop.

More specifically, the operational constraints of a DHS include: 1) heat flow balance and pressure balance equations; and 2) constraints related to mass flow, heat load, and water pressure as presented in (12), (13):

$$\begin{cases} \sum_{j\in\Omega^L}\xi_{j,l}\Phi_{l,t} + P_{l,t}^{CHP}/\eta_h^{CHP} + \eta^{EB}P_{l,t}^{EB} = \Delta\Phi_{l,t} \\ \sum_{i\in\Omega^H} A_{i,l}^H p_{i,t} + \eta^{WP}P_{l,t}^{WP} = \Delta p_{l,t} \end{cases} \tag{12}$$

$$\begin{cases} \sum_{j\in\Omega^L}\xi_{j,l}D_{l,t} = 0; \quad 0 \le D_{l,t} \le \overline{D}_l; \quad \underline{\Phi}_l \le \Phi_{l,t} \le \overline{\Phi}_l \\ \underline{p} \le p_{i,t} \le \overline{p} \quad \forall i \in \Omega^H \end{cases} \tag{13}$$

where $\xi_{j,l}$ marks the relationship between heat pipes *j* and *l*, noting that $\xi_{j,l} = 1$ (-1) when heat pipe *j* is upstream (downstream) of heat pipe *l*, and $\xi_{j,l} = 0$ if heat pipes *j* and *l* are not directly linked; $\bar{D}_l$, $\bar{\Phi}_l$, and $\bar{P}$ are respectively the upper limits of $D_{l,t}$, $\Phi_{l,t}$, and $p_{j,t}$.

E. Proposing the OMEF Model

Overall, the proposed OMEF model can be expressed as:

$$\min_{\left\{P_{u,t}^S, Q_{u,t}^S, F_{q,t}^S, P_{u,t}^{CHP}, P_{u,t}^{EB}, P_{u,t}^{P2G}, P_{u,t}^{WP}, \varepsilon_{wq,t}\right\}} f_t^{\mathrm{OMEF}}$$

$$\text{s.t.} \begin{cases} 0 \le P_{l,t}^{CHP} \le \bar{P}_l^{CHP}; \quad 0 \le P_{u,t}^{EB} \le \bar{P}_u^{EB} \\ 0 \le P_{q,t}^{P2G} \le \bar{P}_q^{P2G}; \quad 0 \le P_{l,t}^{WP} \le \bar{P}_l^{WP} \\ (2)-(5), (11)-(12) \end{cases} \tag{14}$$

where $\bar{P}_u^{CHP}$, $\bar{P}_u^{EB}$, $\bar{P}_u^{P2G}$, and $\bar{P}_u^{WP}$ respectively denote the upper limits of $P_{u,t}^{CHP}$, $P_{u,t}^{EB}$, $P_{u,t}^{P2G}$, and $P_{u,t}^{WP}$. Note that some variables may have different subscripts in different systems; for instance, $P_{u,t}^{CHP}$ and $P_{l,t}^{CHP}$ are the same CHP power generation if the corresponding CHP plant is located at PDS bus *u* and DHS node *l*.

Benefiting from the relaxed loss approximation in (3) and the relaxed gas flow constraints in (5), the proposed OMEF becomes an MIQCP model and can be effectively solved by commercial solvers such as CPLEX [32].

IV. Optimal Expansion Investment Model

The total expansion cost, denoted as f^{Expa}, consists of the planning costs of PDS, GDS, and DHS ($f^{P\tau}$, $f^{G\tau}$, $f^{H\tau}$) at the τ-th planning stage ($\forall\tau\in\Gamma$). In addition to the expansion planning of network topology, which has been studied in [33], [34], the siting and sizing of coupling devices are also accounted for in the proposed model. Moreover, the discrete candidate expansion schemes are considered in the planning model because key parameters such as rating capacity and power cannot change continuously. In this manner, the expansion model is

formulated as:

$$\left\{\begin{matrix}\min\\ x_{u,a}^{P\tau}, x_{k,b}^{G\tau}, x_{l,c}^{H\tau}, y_{u,a}^{P\tau}, y_{k,b}^{G\tau},\\ y_{l,c}^{H\tau}, z_{u,a}^{P\tau}, z_{k,b}^{G\tau}, z_{l,c}^{H\tau}\end{matrix}\right\} f^{\mathrm{Expa}}$$

$$= \sum_{\tau\in\Gamma}(1+\gamma)^{1-\tau}\left(f^{P\tau}+f^{G\tau}+f^{H\tau}\right) \tag{15}$$

$$\text{s.t. } f^{P\tau} = \sum_{u\in\Omega^{NP\tau}}\sum_{a\in\Omega^{PS}}\left(c_1^P S_a + c_2^P \Re_a\right) x_{u,a}^{P\tau}$$

$$+ c_1^P \sum_{u\in\Omega^{P\tau}}\sum_{a\in\Omega^{PS}} S_a y_{u,a}^{P\tau} + c_3^P \sum_{u\in\Omega^{NP\tau}\cup\Omega^{P\tau}}\sum_{a\in\Omega^{EB}} P_a^{EB} z_{u,a}^{P\tau} \tag{16}$$

$$f^{G\tau} = c_1^G \sum_{k\in\Omega^{NW\tau}}\sum_{b\in\Omega^{GS}} F_b x_{k,b}^{G\tau} + c_2^G \sum_{k\in\Omega^{W\tau}}\sum_{b\in\Omega^{GS}} F_b y_{k,b}^{G\tau}$$

$$+ c_3^G \sum_{k\in\Omega^{NW\tau}\cup\Omega^{W\tau}}\sum_{b\in\Omega^{P2G}} P_b^{P2G} z_{k,b}^{G\tau} \tag{17}$$

$$f^{H\tau} = c_1^H \sum_{l\in\Omega^{NL\tau}}\sum_{c\in\Omega^{HS}} D_c x_{l,c}^{H\tau} + c_2^H \sum_{l\in\Omega^{L\tau}}\sum_{c\in\Omega^{HS}} D_c y_{l,c}^{H\tau}$$

$$+ c_3^H \sum_{l\in\Omega^{NL\tau}\cup\Omega^{L\tau}}\sum_{c\in\Omega^{CHP}} P_c^{CHP} z_{l,c}^{H\tau} \tag{18}$$

$$\sum_{\tau\in\Gamma}\sum_{a\in\Omega^{PS}} x_{u,a}^{P\tau} = 1;\ \sum_{\tau\in\Gamma}\sum_{b\in\Omega^{GS}} x_{k,b}^{G\tau} = 1;\ \sum_{\tau\in\Gamma}\sum_{c\in\Omega^{HS}} x_{l,c}^{H\tau} = 1$$

$$\forall u\in\Omega^{NP\tau}, \forall k\in\Omega^{NW\tau}, \forall l\in\Omega^{NL\tau} \tag{19}$$

$$\sum_{a\in\Omega^{PS}} y_{u,a}^{P\tau} \le 1;\ \sum_{b\in\Omega^{GS}} y_{k,b}^{G\tau} \le 1;\ \sum_{c\in\Omega^{HS}} y_{l,c}^{H\tau} \le 1$$

$$\forall u\in\Omega^{P\tau}, \forall k\in\Omega^{W\tau}, \forall l\in\Omega^{L\tau} \tag{20}$$

$$\sum_{\tau\in\Gamma}\sum_{a\in\Omega^{EB}} z_{u,a}^{P\tau} \le 1;\ \sum_{\tau\in\Gamma}\sum_{b\in\Omega^{P2G}} z_{k,b}^{G\tau} \le 1;$$

$$\sum_{\tau\in\Gamma}\sum_{c\in\Omega^{CHP}} z_{l,c}^{H\tau} \le 1$$

$$\forall u\in\Omega^{NP\tau}\cup\Omega^{P\tau}, \forall k\in\Omega^{NW\tau}\cup\Omega^{W\tau}, \forall l\in\Omega^{NL\tau}\cup\Omega^{L\tau} \tag{21}$$

Equations (16)–(18) calculate the expansion costs of the PDS, GDS, and DHS, respectively. Each cost consists of three components, namely the investment in new elements, reinforcement of existing elements, and investment in related coupling devices, respectively. Constraint (19) ensures that duplicate investment is not permitted, while (20) limits the reinforcement times of existing buses, gas pipes, and heat pipes during a planning stage. Constraint (21) enforces that duplicate investment of candidate coupling devices is not allowed.

V. Coordinated Planning Model and an Improved GBD Algorithm

A. Coordinated Planning Model

Based on the proposed operation and expansion sub-models, the coordinated planning model (M_1), is formulated as:

$$\mathrm{M}_1: \begin{cases}\min f^{\mathrm{M1}} = f^{\mathrm{Expa}} \\ \quad + \sum_{\tau\in\Gamma}(1+\gamma)^{1-\tau} d^A \sum_{t\in\Omega^T} f_t^{\mathrm{OMEF}\tau} \\ \text{s.t. } (2)-(5), (12)-(13), (16)-(21)\end{cases} \tag{22}$$

where d^A and Ω^T denote the number of days in one planning stage and the set of daily operation intervals, respectively.

Note that the capacity limits in the OMEF model need to be reformulated to accommodate the binary investment decision variables $\boldsymbol{x}$, $\boldsymbol{y}$, and $\boldsymbol{z}$. Equations (23)–(28) respectively represent the changes in variables $\bar{S}_u$, $\bar{F}_k$, $\bar{D}_l$, P_u^{EB}, P_q^{P2G} and $\bar{P}_l^{CHP}$.

$$\bar{S}_u = \begin{cases}\lambda_u^\tau \sum_{a\in\Omega^{PS}} S_a x_{i,a}^{P\tau} & \forall u\in\Omega^{NP\tau} \\ \lambda_u^\tau \left(S_u^{0\tau} + \sum_{a\in\Omega^{PS}} S_a y_{u,a}^{P\tau}\right) & \forall u\in\Omega^{P\tau}\end{cases} \tag{23}$$

$$\bar{F}_k = \begin{cases}\sum_{b\in\Omega^{GS}} F_b x_{k,b}^{G\tau} & \forall k\in\Omega^{NW\tau} \\ F_k^{0\tau} + \sum_{b\in\Omega^{GS}} F_b y_{k,b}^{G\tau} & \forall k\in\Omega^{W\tau}\end{cases} \tag{24}$$

$$\bar{D}_l = \begin{cases}\sum_{c\in\Omega^{HS}} D_c x_{l,c}^{H\tau} \ \forall l\in\Omega^{NL\tau} \\ D_l^{0\tau} + \sum_{c\in\Omega^{HS}} D_c y_{l,c}^{H\tau} \ \forall l\in\Omega^{L\tau}\end{cases} \tag{25}$$

$$\bar{P}_u^{EB} = \sum_{a\in\Omega^{EB}} P_a^{EB} z_{u,a}^{P\tau} \quad \forall u\in\Omega^{NP\tau}\cup\Omega^{P\tau} \tag{26}$$

$$\bar{P}_q^{P2G} = \sum_{k\in\Omega^{NW\tau}\cup\Omega^{W\tau}} A_{q,k}^G \sum_{b\in\Omega^{P2G}} P_b^{P2G} z_{k,b}^{G\tau}$$

$$\forall q\in\Omega^{NG\tau}\cup\Omega^{G\tau} \tag{27}$$

$$\bar{P}_l^{CHP} = \sum_{c\in\Omega^{CHP}} P_c^{CHP} z_{l,c}^{H\tau} \quad \forall l\in\Omega^{NH\tau}\cup\Omega^{H\tau} \tag{28}$$

where $F_k^{0\tau}$ and $D_l^{0\tau}$ respectively denote the initial gas flow capacity of gas pipe k and water mass flow capacity of heat pipe l at stage τ; and, $S_u^{0\tau}$ and λ_u^τ denote the initial capacity and safety threshold, respectively, of the PDS feeder whose receiving end is bus u.

B. An Improved GBD Algorithm

Based on the proposed formulation, M_1 is a MIQCP model. As an efficient algorithm to solve MIQCP models, the classical GBD is first employed to decompose model M_1 into a master problem M_2 and slave problem M_3 [20], [21], as formulated follows:

$$\mathrm{M}_2: \begin{cases}\min f^{\mathrm{M2}} = f^{\mathrm{Expa}} + \beta \\ \text{s.t. } \begin{cases} f^{\mathrm{M3}} + {B_{\mathrm{cut1}}}^{(m)} \le \beta;\ f^{\mathrm{M4}} + {B_{\mathrm{cut2}}}^{(h)} \le 0 \\ (16)-(21)\end{cases}\end{cases} \tag{29}$$

$$\mathrm{M}_3:\begin{cases}\min\ f^{\mathrm{M3}}=\sum_{\tau\in\Gamma}(1+\gamma)^{1-\tau}d^A\sum_{t\in\Omega^T}f_t^{\mathrm{OMEF}\tau}\\ \text{s.t. }(2)-(5),(12)-(13),(23)-(28)\end{cases}\tag{30}$$

where f^{M2} and f^{M3} denote the objectives of M_2 and M_3, respectively; $B_{cut1}^{(m)}$ and $B_{cut2}^{(\mathrm{h})}$ are the *m*-th optimality Benders cut and the *h*-th feasibility Benders cut, respectively; and β is a non-negative variable.

The GBD is solved in an iterative fashion. In any iteration, M_2 will be solved first to optimize binary variables denoting the expansion of investment decisions. According to the optimized solution to M_2, M_3 is then optimized to minimize the operational cost. However, because M_2 and M_3 are optimized separately, and are interconnected/coordinated by the common binary variables $\{\boldsymbol{x},\boldsymbol{y},\boldsymbol{z}\}$, the optimal solution to M_2 may lead to an infeasible M_3 and thus decrease the efficiency of the GBD. In this paper, a virtual slave problem M_4 is proposed to tackle this issue by introducing nonnegative virtual power, gas, and heat sources (loads), denoted as $P_{u,t}^{VS\tau}(P_{u,t}^{VL\tau})$, $F_{q,t}^{VS\tau}(F_{q,t}^{VL\tau})$, and $\Phi_{l,t}^{VS\tau}(\Phi_{l,t}^{VL\tau})$ respectively, into the first constraints of Equations (2), (4), and (12). Model M_4 is conveniently presented as:

$$\mathrm{M}_4:\begin{cases}\min\ f^{\mathrm{M4}}=\sum_{\tau\in\Gamma}(1+\gamma)^{1-\tau}d^A\sum_{t\in\Omega^T}\left(f_t^{V\tau}\Delta t\right)\\ \quad\text{s.t.}\begin{cases}\text{add virtual sources/loads into }(2),(4),(12)\\ (3),(5),(13),(23)-(28)\end{cases}\end{cases}\tag{31}$$

$$f_t^{V\tau}=\varphi_P\sum_{u\in\Omega^P}\left(P_{u,t}^{VS\tau}+P_{u,t}^{VL\tau}\right)+\varphi_G\sum_{q\in\Omega^G}\left(F_{q,t}^{VS\tau}+F_{q,t}^{VL\tau}\right)+\varphi_H\sum_{l\in\Omega^L}\left(\Phi_{l,t}^{VS\tau}+\Phi_{l,t}^{VL\tau}\right)\tag{32}$$

where $f_t^{V\tau}$ denotes the virtual cost at time *t* in stage τ.

Linear Benders cuts $B_{cut1}^{(\mathrm{m})}$ and $B_{cut2}^{(\mathrm{h})}$ are generated as follows:

$$B_{\mathrm{cut1}}^{(m)}=\sum_{\tau\in\Gamma}\boldsymbol{\sigma_1}\cdot\left[\sum\left(\boldsymbol{x}-\boldsymbol{x}^{(m)}\right),\sum\left(\boldsymbol{y}-\boldsymbol{y}^{(m)}\right),\sum\left(\boldsymbol{z}-\boldsymbol{z}^{(m)}\right)\right]^T\tag{33}$$

$$B_{\mathrm{cut1}}^{(m)}=\sum_{\tau\in\Gamma}\boldsymbol{\sigma_1}\cdot\left[\sum\left(\boldsymbol{x}-\boldsymbol{x}^{(m)}\right),\sum\left(\boldsymbol{y}-\boldsymbol{y}^{(m)}\right),\sum\left(\boldsymbol{z}-\boldsymbol{z}^{(m)}\right)\right]^T\tag{34}$$

where $\sigma_{\mathbf{1}}$ and $\sigma_{\mathbf{2}}$ respectively denote the vectors of the dual multipliers in slave problems M_3 and M_4.

In classical GBD, dual multipliers, i.e., $\boldsymbol{\sigma_1}=\{\boldsymbol{\sigma_1^x},\boldsymbol{\sigma_1^y},\boldsymbol{\sigma_1^z}\}$ and $\boldsymbol{\sigma_2}=\{\boldsymbol{\sigma_2^x},\boldsymbol{\sigma_2^y},\boldsymbol{\sigma_2^z}\}$, remain unchanged throughout the iteration solving process. This may affect the efficiency of generated Benders cuts and the convergence speed. To improve this, a dynamic updating rule for the dual multipliers is proposed in this paper. To further clarify, $\boldsymbol{\sigma_2^x}$ is used as an example to explain the improved algorithm.

Note that M_3 may become infeasible due to insufficient energy distribution capacities (e.g., the capacity of power distribution feeders). In this case, the original GBD algorithm cannot generate a reasonable feasibility cut through a constant $\boldsymbol{\sigma_2^x}$ to deal with the shortage in capacity. The term *reasonable* means the cut reflects the shortage in capacity and helps the algorithm to converge quickly. So, to improve the convergence features, $\boldsymbol{\sigma_2^x}$ should be updated with respect to the capacity shortage. For this purpose, the simulated OMEF of M_4 at the previous (m+h-1)-th iteration is used to update $\boldsymbol{\sigma_2^x}$, which is denoted as $\boldsymbol{\sigma}_{\mathbf{2}^{\boldsymbol{x}(h)}}$, as follows:

$$\boldsymbol{\Theta}_{1\times p}=\begin{bmatrix}\max_{\forall t\in\Omega^T}\left(\sqrt{P_{u,t}^{\tau(m+h-1)^2}+Q_{u,t}^{\tau(m+h-1)^2}}/\lambda_u^\tau\right),\\ \max_{\forall t\in\Omega^T}\left(F_{k,t}^{(m+h-1)}\right),\\ \max_{\forall t\in\Omega^T}\left(D_{l,t}^{(m+h-1)}\right)\end{bmatrix}\tag{35}$$

$$\boldsymbol{\Lambda}_{g\times p}=\exp\left(-\left|\mu\boldsymbol{I}_{g\times1}\boldsymbol{\Theta}_{1\times p}-[\boldsymbol{S}_{1\times g1},\boldsymbol{F}_{1\times g2},\boldsymbol{D}_{1\times g3}]^{\mathrm{T}}\boldsymbol{I}_{1\times p}\right|\right)\tag{36}$$

$$\tilde{\boldsymbol{\Lambda}}_i\Big|_{1\times p}=\begin{cases}\boldsymbol{\Lambda}_i/\max\left(\boldsymbol{\Lambda}_{\langle1:g1\rangle}\right) & \forall i\in[1,2,\ldots,g1]\\ \boldsymbol{\Lambda}_i/\max\left(\boldsymbol{\Lambda}_{\langle g1+1:g1+g2\rangle}\right) & \forall i\in[g1+1,\ldots,g1+g2]\\ \boldsymbol{\Lambda}_i/\max\left(\boldsymbol{\Lambda}_{\langle g1+g2+1:g\rangle}\right) & \forall i\in[g1+g2+1,\ldots,g]\end{cases}\tag{37}$$

$$\boldsymbol{\sigma}_{\mathbf{2}}^{\boldsymbol{x}(h)}{}_j|_{g\times1}=\begin{bmatrix}\boldsymbol{Y}_{g1\times g1}&0&0\\0&\boldsymbol{Y}_{g2\times g2}&0\\0&0&\boldsymbol{Y}_{g3\times g3}\end{bmatrix}\tilde{\boldsymbol{\Lambda}}_j|_{g\times1}\ \forall j\in[1,2,\ldots,p]\tag{38}$$

where Θ, $\boldsymbol{S}$, $\boldsymbol{F}$, and $\boldsymbol{D}$ denote the vectors of maximum capacity at all time slots, transformer capacity, designed natural gas flow, and designed mass flow with dimensions p, g_1, g_2, and g_3, respectively; function max(•) is used to select the largest values; Λ is the intermediate variable and μ is a coefficient, with normalized matrix is $\tilde{\boldsymbol{\Lambda}}$; $\boldsymbol{\Lambda}_{<1:g1>}$ means the sub-matrix of Λ, which takes rows from 1-st to g_1-th; and $\boldsymbol{I}$ and $\boldsymbol{Y}$ are respectively the unit matrix and lower triangular matrix. Note that $g=g_1+g_2+g_3$.

Equation (35) is established to select the maximum required capacities of feeder, gas pipe, and heat pipe for a given day. Then, matrix Θ is compared with the scheme sets $\{\boldsymbol{S},\boldsymbol{F},\boldsymbol{D}\}$ in (36) so as to figure out the deviation between *need & offer*, which is then used to calculate the intermediate variable Λ. Λ is normalized in (37) and used to update $\boldsymbol{\sigma}_{\mathbf{2}^{\boldsymbol{x}(h)}}$ according to (38). Note that the larger the value of $\tilde{\boldsymbol{\Lambda}}_i$ is, the more likely the corresponding scheme is selected. Other dual multipliers can also be updated with the same method.

The improved GBD will proceed through an iterative auction process as described by Algorithm 1.

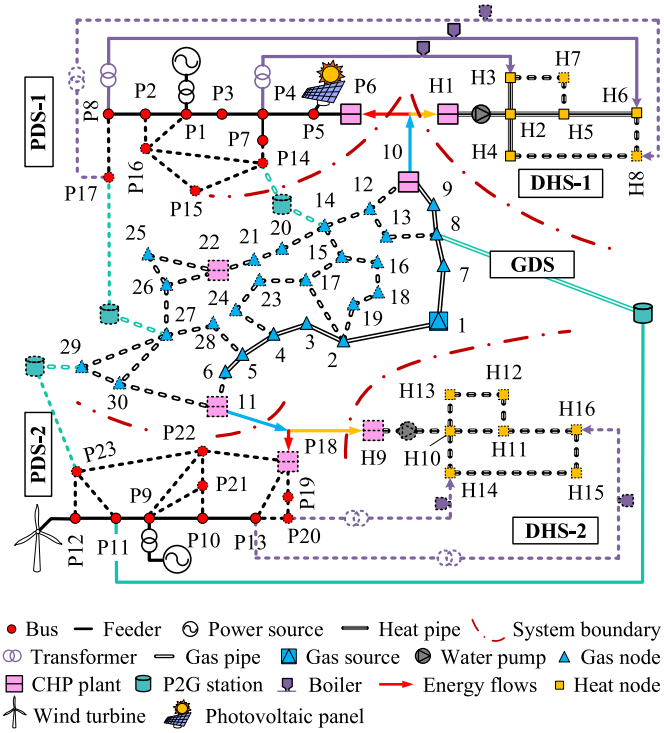

Fig. 3. Initial sample IES.

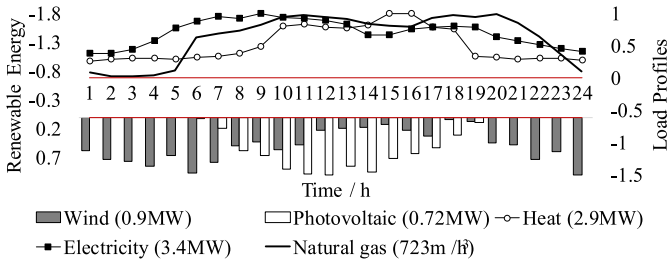

Fig. 4. Normalized daily loads and renewable energy outputs. The maximum values are marked in brackets.

TABLE II
SPECIFIED PARAMETERS OF THE SAMPLE IES

Category	PARAMETERS
PDS & GDS	V_B=10.5 kV; [$\underline{V}$, $\overline{V}$]=[10 kV, 11 kV]
DHS	c=4.168 kJ/(kg·K); κ=1.01 W/(m·K); Υ =0.17; average (T_t^0)=-3 ℃; ρ=960 kg/m^3
Coupling devices	η_e^{CHP}=2 kW/m^3; η_h^{CHP}=0.15; η^{WP}=25.7 kPa/kW; η^{EB}=5; η^{P2G}=0.4 m^3/kW
Operation	φ_P=0.064 \$/(kW·h); φ_G=0.22 \$/m^3; φ_H=0.035 \$/(kW·h); θ_P=0.32 \$/(kW·h); θ_G=0.58 \$/m^3; θ_H=0.35 \$/(kW·h)
Expansion	Γ={1,2,3,4,5}; γ=0.07; μ=1.3

Algorithm 1:

1. Set $f^{\mathrm{M3}} = f^{\mathrm{M4}} = 0$, and $B_{\mathrm{cut1}}^{(0)} = B_{\mathrm{cut2}}^{(0)} = 10^6$.
2. Solve M_2 to obtain its optimization solutions $\{\boldsymbol{x}^*, \boldsymbol{y}^*, \boldsymbol{z}^*\}$.
3. Determine whether or not M_3 is feasible when its binary variables take the values of $\{\boldsymbol{x}^*, \boldsymbol{y}^*, \boldsymbol{z}^*\}$. If so, set $m = m{+}1$, update σ_1 by the method in (35)–(38), and recalculate the values of $\{f^{\mathrm{M3}}, B_{\mathrm{cut1}}^{(m)}\}$.
4. Otherwise, solve problem M_4 instead. Then, set $h = h{+}1$, update σ_2 by the method in (35)–(38), and recalculate the values of $\{f^{\mathrm{M4}}, B_{\mathrm{cut2}}^{(h)}\}$.
5. Judge whether or not the convergence criterion "$B_{\mathrm{cut1}}^{(m)} = B_{\mathrm{cut2}}^{(h)} = 0$" is met. If not, return to **Step 2** and begin the next iteration; else, go to **Step 6**.
6. Output optimal solutions: $\{f^{\mathrm{M2}}, f^{\mathrm{M3}}\}$ and $\{\boldsymbol{x}, \boldsymbol{y}, \boldsymbol{z}, \boldsymbol{P}^{EB}, \boldsymbol{P}^{S}, \boldsymbol{Q}^{S}, \boldsymbol{F}^{S}, \boldsymbol{P}^{P2G}, \boldsymbol{P}^{CHP}, \boldsymbol{P}^{WP}\}$

VI. CASE STUDIES

A. Test Case Description

A case study is carried out to demonstrate the effectiveness of the proposed methodologies. For this sample case, the topologies and specified parameters of PDS and GDS are all available in [22]. Two DHSs are introduced with the physical parameters obtained from [23], [35].

The initial sample IES is shown in Fig. 3, where solid and dotted points/lines respectively denote the existing and candidate devices. Two renewable generators, i.e., a wind turbine and photovoltaic panels, are respectively plugged into existing buses P12 and P5. To begin, two existing PDSs (13 buses and 11 feeders) in the IES and additional candidate devices (10 buses, 19 feeders, and 5 boilers) supply increasing electric power to meet demand. The existing GDS contains 10 gas nodes and 9 gas pipes, with a natural gas source and a CHP plant installed. To extend the GDS, additional new devices could be chosen from 28 new gas nodes as well as 2 potential CHP plants and 3 candidate P2G stations. Additionally, the existing DHS-1 features 6 heat nodes, 10 heat pipes, and 2 boilers. In the near future, DHS-1 should be extended to cover the demands of 8 heat end users. Moreover, another system (DHS-2) is expected to be installed with 8 heat nodes and 9 candidate heat pipes.

In this case, a total planning horizon of 25 years is simulated. The planning horizon is evenly divided into 5 stages, with each stage representing a period of 5 years. It is assumed that the duration days d^A in each stage is 228 days [22]. The average load growths for electricity, natural gas, and heat energy are expected to be 8.2, 6.3, and 4.5%, respectively. Moreover, daily outputs of wind and solar generation are derived from real measured data from Canada [36], as shown in Fig. 4. As per [6], [15]–[18], [35], [37], other specified parameters are set to the values shown in Table II.

B. Effectiveness of the OMEF and Coordinated Planning Models

The optimized planning topologies of the IES at different planning stages are presented in Fig. 5, in which the stages when the feeder/gas pipe/heat pipe is installed are marked in/near the lines. The meanings of the symbols are the same as in Fig. 3.

As the proposed OMEF is an MIQCP model, the well-established commercial solver CPLEX will be employed [32]. The simulation horizon ranges from 0:00 to 24:00 and the time

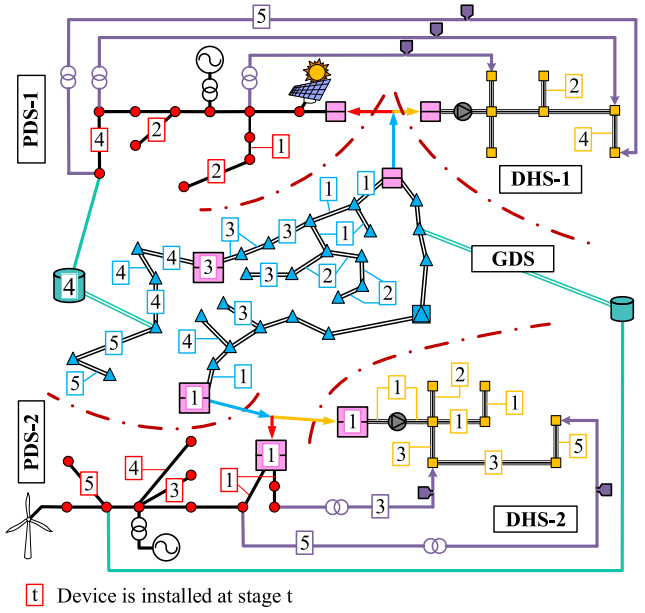

Fig. 5. Extended topologies of the sample IES.

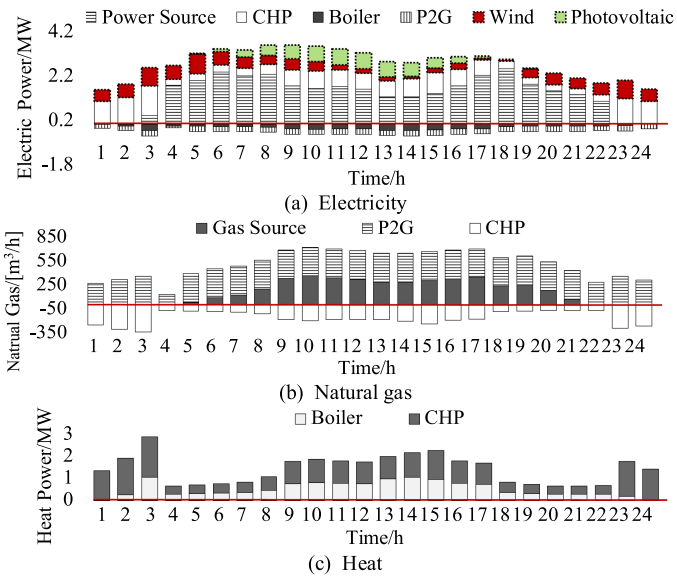

Fig. 6. Daily energy inputs/outputs of the devices in the initial IES.

slot Δt is set to 1 h. When running on a desktop computer with one 1.90 GHz processor (A8-4500 M) and 8 GB of memory, the average computational time is 1.42 s, which varied with different Δt. For instance, when $\Delta t = 15$ min, about 4.69 s is needed for a single simulation.

The optimal daily energy outputs of several devices are presented in consideration of different energies, as shown in Fig. 6. In Fig. 6(b), to consume renewable energies, the P2G station converts more electricity into natural gas. As a result, the CHP plant supplies more electricity and heat demands to balance the natural gas flows in the GDS, as respectively shown in (a) and (c). Consequently, the IES enables a reduction in the amount of energy purchased and saves costs when renewable energies are

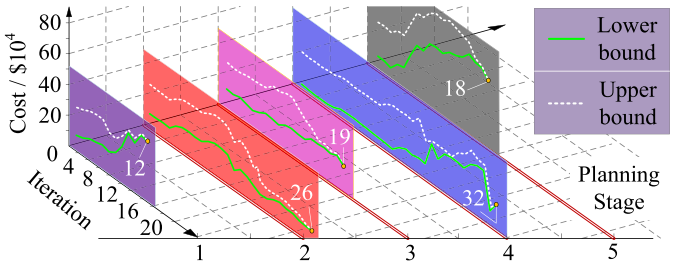

Fig. 7. Upper and lower bounds versus iterations of the improved GBD.

TABLE III
MINIMUM COSTS AT EACH STAGE

Stage	Total [$\times 10^4$ \$]		Detailed costs [$\times 10^4$ \$]					
			PDS	GDS	DHS	Boiler	P2G	CHP
1	**6.58**	O	1.83	0.89	0.77	0.95	0.78	1.36
	71.37	E	41.65	6.32	9.59	--	--	13.81
2	**8.28**	O	1.68	1.51	1.45	1.23	0.89	1.52
	34.77	E	27.33	3.64	3.80	--	--	--
3	**10.19**	O	1.79	2.00	2.11	1.36	1.05	1.88
	65.11	E	18.86	5.72	4.28	1.69	--	34.56
4	**11.10**	O	1.98	2.16	2.08	1.51	1.34	2.03
	49.46	E	39.98	4.56	2.01	--	2.91	--
5	**14.39**	O	2.16	2.61	4.07	1.67	1.57	2.31
	29.64	E	24.72	1.22	2.01	1.69	--	--
Total Cost: 300.89 [$\times 10^4$ \$]								

available in excess. Fig. 6(c) shows the electric boilers are still needed from 2:00 $\sim$ 23:00 when the CHP plant cannot cover all heat demands.

Moreover, for comparison, the absence of all coupling devices will increase the energy purchasing cost from \$3049.84 to \$4418.39 per day. Specifically, the absence of the CHP plant, P2G station, and boilers respectively contribute to 16.69, 73.98, and 9.33% of the total increase in costs.

The optimal planning scheme is obtained from the proposed model M_1 and its improved GBD solution algorithm. The iterative reduction of gaps between the upper and lower bounds are shown in Fig. 7. Take the convergence process at the 2nd planning stage as an example. As shown in Fig. 6, the deviation between the upper and lower bounds at the 2nd planning stage remains constant during the first few rounds of iteration. This is because no feasible solution to model M_3 has yet been found. As the number of iterations grows, M_3 eventually becomes feasible with the help of feasibility cuts generated by the proposed improved GBD algorithm. Thereafter, the deviation between the upper and lower bounds gradually decreases until the convergence criterion is met, i.e., Benders cuts $B_{cut1}^{(m)}$ and $B_{cut2}^{(h)}$ are 0.

The minimum costs at each planning stage in Fig. 5 are respectively listed in Table III, which presents the costs from the aspects of expansion (E) and operation (O) broken down into 6 parts, i.e., the costs of PDS, GDS, DHS, boiler, P2G, and CHP. To supply the ever-growing energy loads, more energy should be delivered through the feeders/pipes, which means that more coupling devices and larger capacities of buses/pipes are badly needed. As a result, the existing buses and heat/gas pipes

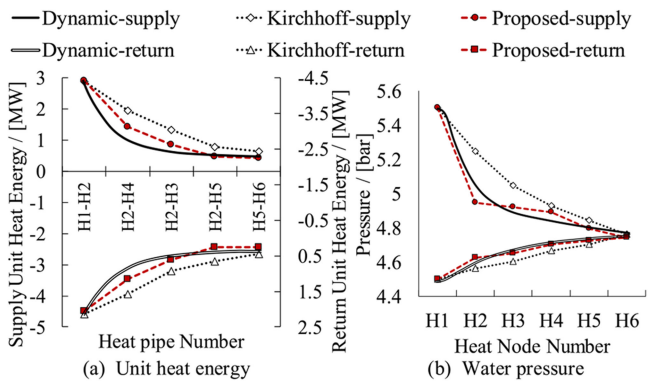

Fig. 8. Comparison of different DHS analytical methods in Case 1.

are enlarged in capacity throughout the planning period. Furthermore, the growing energy demand results in further energy procurement and greater energy losses ($\Delta P_{u,t}$ and $\Delta\Phi_{l,t}$) in energy networks, which is reflected by the increasing operational costs from stage to stage. According to Table III, the expansion of PDS and installation of CHP plants constitute the major share of total expansion investment. For example, stages 1 and 3 have higher expansion costs than other stages, mainly because CHP plants are installed in these two respective stages.

C. Effectiveness of the DHS Steady-State Model

The main contribution of the proposed OMEF model is the development of steady-state heat flow in the DHS. In this section, the effectiveness of the developed heat flow is further investigated.

1) Case 1: Based on the initial DHS in Fig. 3, optimal unit heat energy $\Phi_{l,t}$ ($\forall l \in \Omega^L$) and pressures $p_{i,t}$ ($\forall i \in \Omega^H$) simulated by the dynamic, Kirchhoff-based, and proposed methods are compared. Fig. 8 illustrates the results at 13:00 (i.e., $t = 13$) in detail.

With respect to Fig. 8, three aspects are worthy of more attention:

- All of these methods rely on the same set of physical parameters $\{\Phi^L_{l,t}, D_{l,t}, L_l, d_l, \kappa, \Upsilon, c, \rho, T^0_t\}$.
- Because Fig. 3 employs a radial topology to present the annular DHS, a single heat node/heat pipe actually contains two indicators in Fig. 8, i.e., indicators in the supply and return pipes.
- Detailed formulas of the dynamic method and Kirchhoff-based method are omitted here due to limited space; please refer to [6], [15]–[18] for further details.

The computational time and performance of DHSs based on these methods are further compared in Table IV. Note that the dynamic method is regarded as the benchmark and the accuracy represents the average error compared to the benchmark method in Table IV. The comparisons in Table IV confirm that the proposed model is an effective method for analyzing DHS in the following aspects: 1) compared to the differential dynamic method, the computational complexity is considerably reduced in each run; and 2) compared to the Kirchhoff method, the proposed heat flow considers energy and pressure losses (i.e., $\Delta\Phi_{l,t}$ and $\Delta p_{l,t}$) so as to obtain better accuracy at the cost of a marginal increase in computational burden for a single run. Note that the heat flow in the DHS will be determined about 9000 times in the simulated 5-stage coordinated planning problem. As a result, the proposed method takes significantly less time than the dynamic method while maintaining a satisfactory accuracy, especially compared to the Kirchhoff method.

TABLE IV
COMPARISON OF DIFFERENT DHS ANALYTICAL METHODS

Method	Accuracy	Time per run [s]	Total time [s]	Total cost [$\times 10^4$ \$]
Dynamic	100%	7.06	66131.02	102.91
Kirchhoff	64.53%	1.18	10312.02	143.77
Proposed	85.06%	1.53	13098.33	116.15

*Accuracy is obtained by the grey relational degree analysis [38], which is used to measure the similarity between the curves.

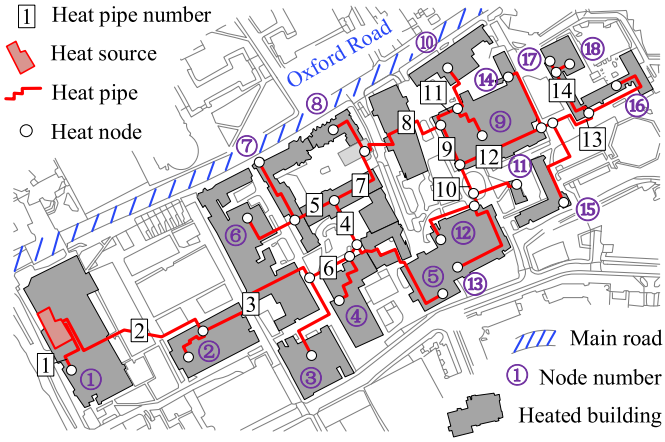

Fig. 9. A larger realistic case of district heating system.

2) Case 2: To double-check the accuracy of the proposed method, the larger realistic DHS at the University of Manchester [6] that has 35 nodes (18 nodes with heat loads) and 68 heat pipes (considers 14 supply and 14 return main pipes) as shown in Fig. 9 is employed.

The proposed heat flow is also compared with the dynamic and Kirchhoff-based methods. To highlight the difference, only the optimal results at the 13-th time slot are presented as an example. The comparisons are demonstrated in Fig. 10. In Fig. 10, the proposed method shows a significant advantage in improving accuracy when compared to the present Kirchhoff-based method, benefitting from the consideration of the physical relationship between heat and pressure. If the dynamic method is employed as a benchmark (i.e., 100% accuracy), the accuracies of the Kirchhoff-based and proposed methods are respectively 63.41 and 82.77%.

D. Effectiveness of the Improved GBD Algorithm

Compared to classical GBD, the improved algorithm shows great advantages in terms of saving computational time. Table V shows that a smaller number of iterations is required for the

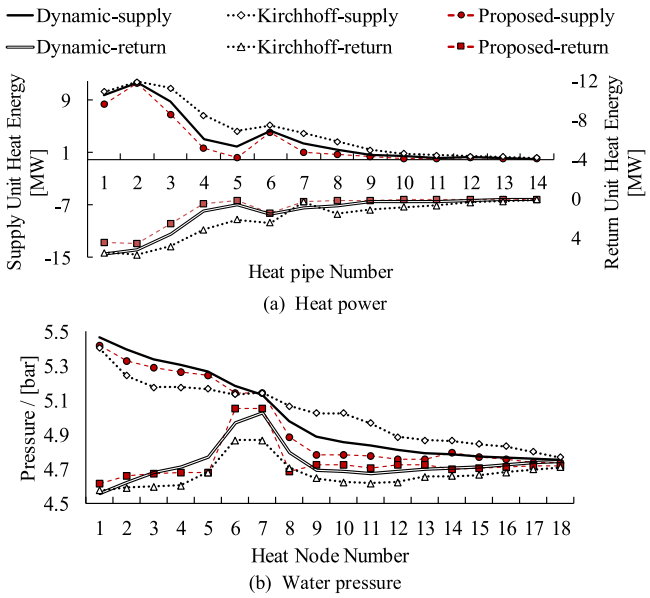

Fig. 10. Comparison of different DHS analytical methods in Case 2. Numbers of heat pipes and heat nodes are as shown in Fig. 9.

TABLE V
COMPARISON BETWEEN IMPROVED AND CLASSICAL GBDS

Algorithm		Iterations at each stage					Total time [s]	Total cost [$\times 10^4$ $]
		1	2	3	4	5		
Classical GBD		28	35	27	50	34	33118.72	300.90
Improved GBD	μ=0.3	25	35	23	39	28	35905.29	300.95
	μ=0.5	19	30	20	36	22	30399.81	300.98
	μ=1.0	14	27	19	33	20	27048.65	300.88
	μ=1.3	12	26	19	32	18	25612.44	300.89
	μ=1.5	13	28	21	32	21	27527.39	300.92
	μ=2.0	17	32	24	35	24	31596.66	300.88
	μ=2.3	20	34	24	38	28	34469.08	300.89

improved GBD algorithm to converge compared to the classical GBD. For each planning stage, the improved GBD (when $\mu = 1.3$) requires 16, 9, 8, 18, and 16 fewer iterations than the classical GBD, respectively. This feature also leads to a significant reduction in total computational time (7506 s reduction), which reflects a considerable boost in computational efficiency. Benefit from the proposed dynamic dual multipliers to update feasibility cuts, the improved GBD is capable of generating cutting planes with respect to the amount of capacity shortage, which will be further considered in searching for the optimal solution. In contrast, classical GBD cannot effectively identify the capacity shortage and tends to cover for it using lines/pipes/coupling devices with random capacities. Therefore, the convergence of the improved GBD speeds up the process even further.

In Table V, the sensitivity of μ is also analyzed. The value of μ reflects the balance between optimality and feasibility when searching for the optimal solution. If a small μ is selected (e.g., $\mu < 1.3$ in Table V), the optimality of the problem, i.e., the planning cost in this paper, has a higher priority than feasibility. Thus, the improved GBD tends to select candidate schemes with small costs and capacities. On the other hand, a larger μ (e.g., $\mu > 1.3$ in Table V) is employed, the improved GBD emphasizes on the feasibility of the planning problem and candidate schemes with large capacities and costs will be preferred during the search. As a result, the improved GBD takes more iterations to converge when μ is either very small or very large to find the optimal feasible solution. As shown in Table V, the improved GBD is most computational efficient when $\mu = 1.3$, which means the corresponding search pattern results in the fastest convergence speed in the simulated test case. Note that varying the value of μ does not have considerable influences on the optimized total cost as shown in Table V. Hence, the proposed improved GBD algorithm can effectively find the global optimal solution.

TABLE VI
PLANNING RESULTS FOR TWO DIFFERENT CASES

Case	Total [$\times 10^4$ $]	Classification	Selected Devices	Costs [$\times 10^4$ $]	
				Operational	Expansion
3	**26.19 (O)**	PDS	7-8-12-13	10.58	92.64
		GDS	1-3-5	3.89	40.83
		DHS	17	11.72	18.07
	151.54 (E)	Boiler	--	--	--
		P2G	--	--	--
		CHP	--	--	--
4	**22.18 (O)**	PDS	7-9-12-10	7.31	74.40
		GDS	1-2-4	4.49	32.17
		DHS	17	2.83	12.96
	148.94 (E)	Boiler	16-19	1.36	4.54
		P2G	6-15	2.77	11.22
		CHP	21-22-23	3.42	13.65

E. The Necessity of Coordinated Planning

The simulation results in the previous sections validate the feasibility and effectiveness of the coordinated planning strategy while making no attempt to discuss its necessity. As shown in Fig. 11, a realistic large-scale IES at the University of Manchester [6] is extended through the coordinated and uncoordinated planning methods, respectively. At present, this IES has a scale of 54 buses, 59 gas nodes, and 35 heat nodes. In the coming planning stage (5 years), one CHP plant, one P2G station, two boilers, eight buses, nine gas nodes, and two heat nodes should be installed to meet increasing energy demands.

For comparison, uncoordinated planning is denoted as Case 3, where PDS, GDS, and DHS are considered as independent systems and are not coupled. In other words, no coupling devices need to be installed in Case 3. Besides, due to the absence of CHP plants, Case 3 should procure heat energy from an outside source. The proposed coordinated planning is denoted as Case 4. The parameters remain the same as discussed in Table II and [6].

The planning results of these two cases are compared in Table VI. As expected, coupling devices markedly impact the optimal topology of the IES. Case 4 has a lower cost (save \$ 6.61×10^4) even though the additional installation costs of coupling devices are accounted for. The expansion (E) costs of PDS, GDS, and DHS in Case 3 are all higher than those of Case 4. In terms of operational (O) costs, Case 4 allows end-users to be supplied in a more cost-effective way. Specifically, due

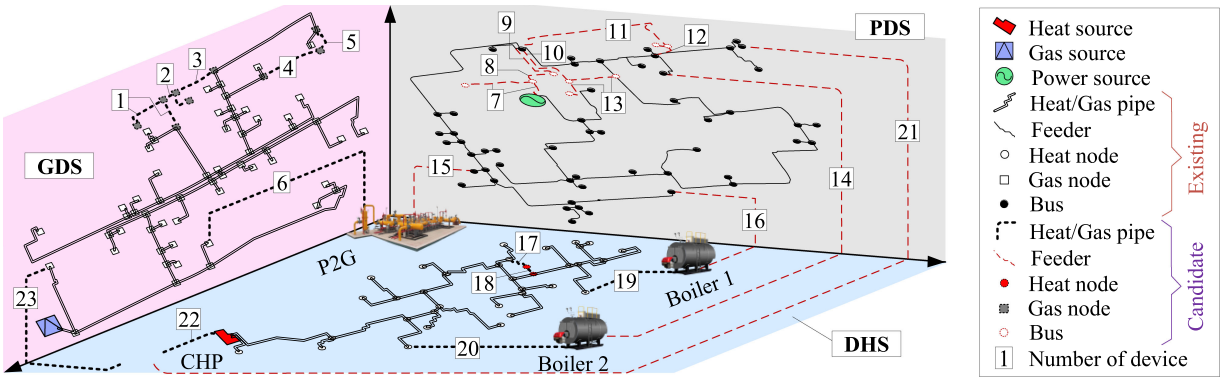

Fig. 11. A realistic large-scale sample IES at The University of Manchester. The candidate devices involved are designed to facilitate the comparison.

to the absence of CHP plants in Case 3, more electricity is consumed and more power flows through the PDS to supply the heat load, which leads to a higher operational cost for the PDS. Similarly, the demand for hot water supply in the DHS is also increased in Case 3. But, the significant cost growth in operating DHS is mainly caused by the procurement of heat energy. In contrast, the burden on the GDS is lower in Case 3 due to the absence of CHP plants. Nonetheless, the total operational cost of Case 3 is still significantly higher than that of Case 4.

In summary, the comparison of Case 3 (uncoordinated planning) and Case 4 (coordinated planning) shows that the coordinated strategy has great advantages for the planning of IES, both in terms of operational and expansion costs.

VII. Conclusion

This paper presents a coordinated planning model for the expansion of IESs in a district energy sector. The proposed model consists of an operation sub-model, i.e., the OMEF model, and an expansion sub-model. An improved GBD is developed to efficiently solve the proposed planning model. Five planning stages are considered in the case studies, and the numerical results verify the effectiveness of the coordinated planning of IESs and the computational efficiency of the improved GBD algorithm. Compared to energy systems that are planned independently, the coordination of various energy systems in the planning phase is shown to achieve lower investment and operational costs.

The following issues will be addressed in the future:

- Modeling of heat storage equipment to expand the OMEF model presented in this work and include more feasible operation modes of IESs.
- Inclusion of intelligent traffic networks with various kinds of electric vehicles in the coordinated expansion planning of IESs and charging infrastructures.
- Expected development of this methodology as a software package for application in industrial parks.

References

[1] M. J. Sanjari, H. B. Gooi, and N. Nair, "Power generation forecast of hybrid PV-wind system," *IEEE Trans. Sustain. Energy*, to be published, doi: 10.1109/TSTE.2019.2903900.

[2] S. Córdova, H. Rudnick, Á. Lorca, and V. Martínez, "An efficient forecasting-optimization scheme for the intraday unit commitment process under significant wind and solar power," *IEEE Trans. Sustain. Energy*, vol. 9, no. 4, pp. 1899–1909, Oct. 2018.

[3] Y. Dai, L. Chen, Y. Min, Q. Chen, J. Hao, K. Hu, and F. Xu, "Dispatch model for CHP with pipeline and building thermal energy storage considering heat transfer process," *IEEE Trans. Sustain. Energy*, vol. 10, no. 1, pp. 192–203, Jan. 2019.

[4] D. Alkano and J. M. A. Scherpen, "Distributed supply coordination for power-to-gas facilities embedded in the energy grids," *IEEE Trans. Smart Grid*, vol. 9, no. 2, pp. 1012–1022, Mar. 2018.

[5] M. Zhang, C. Xu, X. Du, M. Amjad, and D. Wen, "Off-design performance of concentrated solar heat and coal double-source boiler power generation with thermocline energy storage," *Appl. Eng.*, vol. 189, pp. 697–710, Mar. 2017.

[6] X. Liu and P. Mancarella, "Modelling, assessment and Sankey diagrams of integrated electricity-heat-gas networks in multi-vector district energy systems," *Appl. Eng.*, vol. 167, pp. 336–352, Apr. 2016.

[7] B. Odetayo, M. Kazemi, J. MacCormack, W. D. Rosehart, H. Zareipour, and A. R. Seifi, "A chance constrained programming approach to the integrated planning of electric power generation, natural gas network and storage," *IEEE Trans. Power Syst.*, vol. 33, no. 6, pp. 6883–6893, Nov. 2018.

[8] T. Ding, Y. Hu, and Z. Bie, "Multi-stage stochastic programming with nonanticipativity constraints for expansion of combined power and natural gas systems," *IEEE Trans. Power Syst.*, vol. 33, no. 1, pp. 317–328, Jan. 2018.

[9] B. Zhao, A. J. Conejo, and R. Sioshansi, "Coordinated expansion planning of natural gas and electric power systems," *IEEE Trans. Power Syst.*, vol. 33, no. 3, pp. 3064–3075, May 2018.

[10] Q. Zeng, B. Zhang, J. Fang, and Z. Chen, "A bi-level programming for multistage co-expansion planning of the integrated gas and electricity system," *Appl. Eng.*, vol. 200, pp. 192–203, Aug. 2017.

[11] S. Klyapovskiy, S. You, H. Cai, and H. W. Bindner, "Integrated planning of a large-scale heat pump in view of heat and power networks," *IEEE Trans. Indus. Appl.*, vol. 55, no. 1, pp. 5–15, Jan.–Feb. 2019.

[12] F. Wang, H. Liu, Y. Chen, J. Wu, B. Yang, and W. Ruan, "Optimal co-planning of park-level integrated heat and electricity energy systems," in *Proc. Int. Conf. Electric Power Energy Convers. Syst.*, Kitakyushu, Japan, Apr. 2018.

[13] W. Huang, N. Zhang, J. Yang, Y. Wang, and C. Kang, "Optimal configuration planning of multi-energy systems considering distributed renewable energy," *IEEE Trans. Smart Grid*, vol. 10, no. 2, pp. 1452–1464, Mar. 2019.

[14] F. Marty, S. Serra, S. Sochard, and J. M. Reneaume, "Simultaneous optimization of the district heating network topology and the organic rankine cycle sizing of a geothermal plant," *Energy*, vol. 159, pp. 1060–1074, Sep. 2018.

[15] J. Zheng, Z. Zhou, J. Zhao, and J. Wang, "Function method for dynamic temperature simulation of district heating network," *Appl. Therm. Eng.*, vol. 123, pp. 682–688, Aug. 2017.

[16] M. Vesterlund, A. Toffolo, and J. Dahl, "Optimization of multi-source complex district heating network, a case study," *Energy*, vol. 126, pp. 53–63, May 2017.

[17] X. Liu, J. Wu, N. Jenkins, and A. Bagdanavicius, "Combined analysis of electricity and heat networks," *Appl. Eng.*, vol. 162, pp. 1238–1250, Jan. 2016.
[18] J. Dorfner and T. Hamacher, "Large-scale district heating network optimization," *IEEE Trans. Smart Grid*, vol. 5, no. 4, pp. 1884–1891, Jul. 2014.
[19] Y. Wen, X. Qu, W. Li, X. Liu, and X. Ye, "Synergistic operation of electricity and natural gas networks via ADMM," *IEEE Trans. Smart Grid*, vol. 9, no. 5, pp. 4555–4565, Sep. 2018.
[20] H. Zhang, S. J. Moura, Z. Hu, W. Qi, and Y. Song, "Joint PEV charging network and distributed PV generation planning based on accelerated generalized benders decomposition," *IEEE Trans. Transp. Electrific.*, vol. 4, no. 3, pp. 789–803, Sep. 2018.
[21] Z. Yuan and M. R. Hesamzadeh, "A modified benders decomposition algorithm to solve second-order cone ac optimal power flow," *IEEE Trans. Smart Grid*, vol. 10, no. 2, pp. 1713–1724, Mar. 2019.
[22] C. A. Saldarriaga, R. A. Hincapié, and H. Salazar, "A holistic approach for planning natural gas and electricity distribution networks," *IEEE Trans. Power Syst.*, vol. 28, no. 4, pp. 4052–4063, Nov. 2013.
[23] J. Huang, Z. Li, and Q. H. Wu, "Coordinated dispatch of electric power and district heating networks: A decentralized solution using optimality condition decomposition," *Appl. Eng.*, vol. 206, pp. 1508–1522, Nov. 2017.
[24] W. Gu, J. Wang, S. Lu, Z. Luo, and C. Wu, "Optimal operation for integrated energy system considering thermal inertia of district heating network and buildings," *Appl. Eng.*, vol. 199, pp. 234–246, Aug. 2017.
[25] L. Huang, Y. Fu, Y. Mi, J. Cao, and P. Wang, "A markov-chain-based availability model of offshore wind turbine considering accessibility problems," *IEEE Trans. Sustain. Energy*, vol. 8, no. 4, pp. 1592–1600, Oct. 2017.
[26] H. G. Yeh, D. F. Gayme, and S. H. Low, "Adaptive VAR control for distribution circuits with photovoltaic generators," *IEEE Trans. Power Syst.*, vol. 27, no. 3, pp. 1656–1663, Aug. 2012.
[27] J. Fang, Q. Zeng, X. Ai, Z. Chen, and J. Wen, "Dynamic optimal energy flow in the integrated natural gas and electrical power systems," *IEEE Trans. Sustain. Energy*, vol. 9, no. 1, pp. 188–198, Jan. 2018.
[28] W. Liu, J. Zhan, C. Y. Chung, and Y. Li, "Day-ahead optimal operation for multi-energy residential systems with renewables," *IEEE Trans. Sustain. Energy*, vol. 10, no. 4, pp. 1927–1938, Oct. 2019.
[29] Naturalgas, "The transportation of natural gas." [Online]. Available: https://web.archive.org/web/20110101062510/, http://naturalgas.org/naturalgas/transport.asp
[30] Z. Shi, L. Liu, P. Xiao, Z. Geng, and G. Fang, "Applying transmission line theory to study the transmitting turn-off current in a long grounded wire," *IEEE Trans. Antennas Prop.*, vol. 65, no. 10, pp. 5112–5122, Oct. 2017.
[31] Z. Azizi, A. Alamdari, and M. R. Malayeri, "Thermal performance and friction factor of a cylindrical microchannel heat sink cooled by Cu-water nanofluid," *Appl. Therm. Eng.*, vol. 99, pp. 970–978, Apr. 2016.
[32] IBM, "CPLEX Optimizer," [Online]. Available: https://www.ibm.com/analytics/cplex-optimizer
[33] W. Yao, C. Y. Chung, F. Wen, M. Qin, and Y. Xue, "Scenario-based comprehensive expansion planning for distribution systems considering integration of plug-in electric vehicles," *IEEE Trans. Power Syst.*, vol. 31, no. 1, pp. 317–328, Jan. 2016.
[34] A. Zare, C. Y. Chung, J. Zhan, and S. O. Faried, "A distributionally robust chance-constrained MILP model for multistage distribution system planning with uncertain renewables and loads," *IEEE Trans. Power Syst.*, vol. 33, no. 5, pp. 5248–5262, Sep. 2018.
[35] C. Wu, W. Gu, P. Jiang, Z. Li, H. Cai, and B. Li, "Combined economic dispatch considering the time-delay of district heating network and multi-regional indoor temperature control," *IEEE Trans. Sustain. Energy*, vol. 9, no. 1, pp. 118–127, Jan. 2018.
[36] Natural Resources Canada, "Solar resource data available for Canada-SUNY (free)," [Online]. Available: https://www.nrcan.gc.ca/energy/renewable-electricity/solar-photovoltaic/14390
[37] Y. Li *et al.*, "Optimal stochastic operation of integrated low-carbon electric power, natural gas, and heat delivery system," *IEEE Trans. Sustain. Energy*, vol. 9, no. 1, pp. 273–283, Jan. 2018.
[38] A. Acır, M. E. Canlı, İ. Ata, and R. Çakıroğlu, "Parametric optimization of energy and exergy analyses of a novel solar air heater with grey relational analysis," *Appl. Therm. Eng.*, vol. 122, pp. 330–338, Jul. 2017.

Wentao Yang (S'19) received the B.E. degree in electrical engineering from Wuhan University, Wuhan, China, in 2015. He is currently working toward the Ph.D. degree in Zhejiang University, Hangzhou, China. His main research interests include electrical vehicles, integrated energy systems, and transactive energy.

Weijia Liu received the B.Eng. and Ph.D. degrees in electrical engineering from Zhejiang University, Hangzhou, China, in 2011 and 2016, respectively.

He is currently a Researcher with National Renewable Energy Laboratory, Golden, CO, USA. His research interests include smart grid, integrated energy systems, and transactive energy.

Chi Yung Chung (M'01–SM'07–F'16) received the B.Eng. (Hons.) and Ph.D. degrees in electrical engineering from The Hong Kong Polytechnic University, Hong Kong, China, in 1995 and 1999, respectively.

He is currently a Professor, the NSERC/SaskPower (Senior) Industrial Research Chair in Smart Grid Technologies, and the SaskPower Chair in Power Systems Engineering with the Department of Electrical and Computer Engineering, University of Saskatchewan, Saskatoon, SK, Canada.

Dr. Chung is an Editor for the IEEE TRANSACTIONS ON POWER SYSTEMS, IEEE TRANSACTIONS ON SUSTAINABLE ENERGY, and IEEE POWER ENGINEERING LETTERS. He is also an IEEE PES Distinguished Lecturer and a Member-at-Large (Global Outreach) of the IEEE PES Governing Board.

Fushuan Wen received the B.E. and M.E. degrees from Tianjin University, Tianjin, China, in 1985 and 1988, respectively, and the Ph.D. degree from Zhejiang University, Hangzhou, China, in 1991, all in electrical engineering. He joined the Faculty of Zhejiang University in 1991. He has been a Full Professor and the Director of the Institute of Power Economics and Information since 1997, and the Director of Zhejiang University-Insigma Joint Research Center for Smart Grids since 2010. He was a University Distinguished Professor, the Deputy Dean of the School of Electrical Engineering, and the Director of the Institute of Power Economics and Electricity Markets with the South China University of Technology, Guangzhou, China, from 2005 to 2009. From May 2014 to May 2017, he was a Professor with Universiti Teknologi Brunei, Brunei. His research interests include power industry restructuring, power system alarm processing, fault diagnosis and restoration strategies, as well as smart grids and electric vehicles.

Prof. Wen is an Editor for the IEEE TRANSACTIONS ON POWER SYSTEMS and IEEE POWER ENGINEERING LETTERS, a Subject Editor on power system economics for *IET Generation, Transmission and Distribution*, and an Associate Editor for the *Journal of Energy Engineering (ASCE)* and the *Journal of Modern Power Systems and Clean Energy (Springer)*.